Boron-Doped Hydroxyapatite Coatings on NiTi Alloys Using the Electrophoretic Deposition Method: Enhanced Corrosion and Adhesion Performances

M.E. Aksoy, B. Aksakal, N. Aslan, and B. Dikici

Metallic implants are functionalized with coatings due to the need to protect against biological corrosion in the body. Hydroxyapatite (HAp) has desirable biocompatibility and structural properties, but poor mechanical properties limit its use as a standalone coating. In this study, boron-doped hydroxyapatite (B-HAp) biocomposites containing 5, 10, and 15% boron by weight were synthesized by the sol-gel method and applied as a coating to NiTi using electrophoretic deposition (EPD). The deposition was carried out for 60, 90, and 120 s, and sintering at 750 °C for 75 minutes under vacuum. The coated substrates were then characterized by XRD, SEM, and FT-IR, and their adhesion strengths and *in-vitro* corrosion behaviors in simulated body fluid were compared with uncoated samples. The results showed that the microporous powders formed well-bonded structures, which positively affect adhesion strength. The highest adhesion strength (30 MPa) and corrosion resistance were achieved with 15 wt.% B-HAP coating at 120 s deposition time and 76.5 µm coating thickness.

1. Introduction

A synthesized material's lifetime in the body usually depends on its biocompatibility and capacity for osseointegration with hard tissue (Ref 1). Disadvantages of the metals used in biomaterials include being harder than tissues, having high density, being bioinert, suffering from corrosion, and releasing metal ions that may cause allergic tissue reactions (Ref 2, 3). The effects of poor osseointegration and development of undesired surface properties due to biologic corrosion can vary, but may result in looseness, pain, and need for re-operation (Ref 4, 5). Compared to some other commonly used implant materials, Nitinol (NiTi) alloys have better biocompatibility, superelasticity, and shape memory effect; accordingly, these alloys have a wide range of applications in cardiovascular, orthopedic, and dental, such as dental archwires, heart valves, spinal rods, and vertebral spacers, knee prosthesis components, plates for fractured bones, and stent applications (Ref 6). However, while the mechanical aspects of NiTi alloys may be reasonably predictable, long-term corrosion and surface degradation remain critical challenges for the implant market.

Namely, contact between NiTi and hard tissues may lead to possible Ni-ion release and allergic reactions, posing a risk to cell development. Improving overall biocompatibility and corrosion resistance, and also minimizing the potential for allergic reactions, is therefore of great interest for biomedical applications (Ref 7). Accordingly, performing several protective surface treatments and creating a passive layer on the surface has become important for most clinical applications using NiTi (Ref 8). Huang *et al.* (Ref 9) studied the surface characteristics and corrosion response of several commercial archwires and observed significant differences, with some showing relatively poor pitting and crevice corrosion resistance especially in lower-pH environments.

Bioceramic materials, especially HAp, are likewise limited in use by factors such as the occurrence of cracks, low mechanical strength, and difficulty in implantation. Developing HAp coatings for NiTi material that incorporate additives and reinforcing materials could minimize or even overcome the poor mechanical properties of pure HAp (Ref 10, 11). In particular, studies conducted on boron (B) doped HA-based bio-composite powder have reported that boron and its compounds have important roles in bone healing and osteogenesis (Ref 12-14). This may be especially important in the context of rheumatoid arthritis, where bone boron content is less than in healthy bones (Ref 15). Several processes are used in applying coatings to metallic surfaces such as sol-gel method (Ref 16-19), plasma spraying (Ref 20), electrophoretic deposition (Ref 21), anodic oxidation (Ref 22), spark plasma sintering (Ref 23), hydrothermal (Ref 24) and plasma electrolytic oxidation methods (Ref 25). Among such methods, electrophoretic deposition (EPD) has the advantages of easy installation, low hardware cost, applicability to complex shapes, and allowing the checking of coating thickness (Ref 26, 27). Besides, the EDP method has a high deposition rate as compared to the many coating methods and no binder required. Another advantage of the EPD is that the coating thickness and

M.E. Aksoy, Institute of Post Graduate Education, Munzur University, 62000 Tunceli, Turkey; **B. Aksakal**, Department of Metallurgical and Materials, Yildiz Technical University, 34220 Istanbul, Turkey; **N. Aslan**, Department of Metallurgical and Materials, Munzur University, 62000 Tunceli, Turkey; and **B. Dikici**, Department of Metallurgical and Materials Engineering, Ataturk University, 25240 Erzurum, Turkey. Contact e-mails: baksakal2@gmail.com and baksakal@yildiz.edu.tr.

morphology can be controlled by using electrochemical parameters (Ref 28).

In the literature, although various studies have been carried out to demonstrate the synthesis, structural and morphological properties of boron-doped calcium phosphate based biocomposite powders (Ref 29). However, NiTi metallic implants have not been studied in detail. Unlike the literature, in this work, different proportions (5, 10 and 15% by weight) of boron ion-doped hydroxyapatite-based biocomposite powders were produced, and then biocomposite coatings were applied on biomedical Nitinol (NiTi) alloys for different durations (60, 90 and 120 seconds) with the EPD method. In addition to the effect of boron additive on structural and morphological properties, the effects of adhesion strength, in-vitro corrosion resistance, coating thickness on adhesion strength have been extensively studied.

2. Experimental Procedures

2.1 Substrate Material

NiTi alloys were commercially procured in $0.3 \times 250 \times 250$ mm sizes in compliance with the ASTM F2063 standard (Allotech Ind, China) and then machined into samples having dimensions of 10×15 mm. As the surface roughness of metallic implants has a significant effect on adhesion and the degree of osseointegration, providing biomechanical fixation (Ref 30, 31), the substrate surfaces were sandblasted with silicon dioxide (SiO_2) sand (300 μm) to impart a rough structure. After sandblasting, the samples were cleaned in an ultrasonic cleaning device (Bandelin Sonorex, RK31H).

2.2 Synthesis of Boron-Doped Bioceramic (B–HAp)

Boron-doped HAp powders (B–HAp) of differing proportions (5, 10, and 15 wt.% B) were synthesized from HAp (<25 μm, Nanograph) with 99% purity and H_3BO_3 (<25 μm, Merck) using a simple chemical "acid-base" method for obtaining bioceramic coatings on NiTi implant materials. Firstly, H_3BO_3 was added to pure water in a magnetic mixer (Mtops HS12, 1500 rpm) together with dissolved HAp. As the addition of H_3BO_3 caused aggregates to form, the mixture was mechanically milled to an average particle size of 15 μm. Then, to keep the pH at 7.40, sodium hydroxide (NaOH, Merck) was added and the solution aged for 12 h, followed by homogenization for 7 min in an ultrasonic homogenizer (Sonic-VC 505, 750 W). After the aging process, the synthesized biocomposite powders (15 μm) were sintered under vacuum (MSE Furnace, 1500°C), then dried overnight in an oven at 130°C (Binder ED23). The presence of H_3BO_3 in boron-doped (B-HAp) powders was confirmed by X-ray diffraction (XRD, Rigaku -MiniFlex 600) and Fourier transform IR (FT-IR) spectroscopy (JASCO - 6700, KBr mode).

2.3 Preparation of Suspensions for EPD

Suspensions for the EPD coating of specimen groups (only-HAp and 5, 10, 15 wt.% B-HAp) were prepared using N, N-dimethylformamide (Isolab, 99%), and ethanol (Merck, 99.9%). Briefly, suspensions were mixed ultrasonically for 25 min in a magnetic mixer and then homogenized for 5 minutes at 20 kHz in a homogenizer. A previous study reported an increase in electrical conductivity when iodine was added to the suspension (Ref 31, 32); and here, after homogenization, 0.01M iodine was added to all suspensions.

2.4 EPD Process and Sintering

The assembly for performing EPD was set up with a DC power supply. Samples were placed in the anode and countering cathode with a stainless-steel plate for the sample groups. For all coating types (only-HAp and 5, 10, and 15 wt.% B-HAp), biocomposite coatings were applied to the NiTi substrates connected to the cathode. The EPD process was optimized, with the optimal process parameters determined as 150 V and 60, 90, or 120 s deposition time with a 10 mm fixed electrode distance. The EPD deposition times and film thicknesses achieved for each coating type are tabulated in Table 1.

Hereafter, as given in Table 1, the coatings are referred to as N_n for easy expression of the coating time and B ratio. For example, N_4 describes the sample in which NiTi was coated with 5 wt.% B-HAp biocomposite for 60 s deposition time. The coated samples were left to dry for 24 h under room conditions, then further dried for 2 h at 130°C in preparation for sintering. Sintering was carried out in a vacuum atmosphere for 75 min at 750°C. After completion of sintering, all samples were stored in a desiccator for characterization, analysis, and testing.

2.5 Adhesion Tests

The adhesion strength of the biocomposite coatings applied to metallic sample surfaces was tested via the ISO 13779-2 standard, consisting of a pull-out test performed with a specially designed die-apparatus mounted on the jaws of a pulling device. NiTi rods (8×15 mm) were used as the substrate for all groups. DP420 epoxy (3M - Turkey) type adhesive was applied to the butts of the rods, whose adhesion zones corresponded to 50 mm^2 cross sections, and then each coated sample was placed in a die at a right angle to the surface axis to prevent axial leakage. The adhesive was dried for 12 h at room temperature (25°C) and then for an additional 4 h in an oven at 130°C. Afterward, adhesion tests were performed at a tensile speed of 1 mm·min^{-1} (Shimadzu, 100 kN). Experiments were repeated four times, and the results are presented as averages with standard error values (OriginPro 2015 SR2, Northampton, MA). Groups were compared in terms of adhesion strength-elongation (%) with t tests used to determine significant differences, taking a p value less than 0.05 as a statistically significant value.

2.6 In-vitro Corrosion Tests

Corrosion tests were performed with a potentiostat/galvanostat (Gamry, PCI14/750) in simulated body fluid (SBF) at 37 °C. During polarization tests, a silver/silver chloride electrode (Ag/AgCl) was used as the KBr-reference electrode, and platinum (Pt) wire and coated samples were used as the counter and working electrodes, respectively. SBF, prepared according to Kokubo's protocol (Ref 33), was used in corrosion testing due to its ion concentration values being similar to those of blood plasma (Table 2). Samples were immersed in the SBF until a steady-state open circuit potential (OCP) was obtained, after which the potentiodynamic scanning (PDS) test was started at the cathodic overpotential, proceeding at a rate of 1 mV·s^{-1} until reaching the 0.2 V anodic overpotential. Electro-

Table 1　Coating groups and film thicknesses (µm) with sample ID

EPD-coating time, s	Only-HA	5 wt% B–HA	10 wt% B–HA	15 wt% B–HA
60	N_1	N_4	$\mathbf{N_7}$	N_{10}
	23 µm ±0.6	28.1 µm ±1.4	42.3 µm ±4.3	48.3 µm ±2.8
90	N_2	N_5	N_8	N_{11}
	27 µm ±1.1	31.8 µm ±4.4	48.8 µm ±3.9	51.1 µm ±2.0
120	N_3	N_6	$\mathbf{N_9}$	$\mathbf{N_{12}}$
	29.7 µm ±1.2	38.7 µm ±2.6	53.7 µm ±3.6	76.5 µm ±2.8

Table 2　Comparison of blood plasma and simulated body fluid (SBF) ion concentration for 10^{-3} moles (Ref 21)

Ion	Blood plasma	Simulated body fluid (SBF)
Na^+	142	142
K^+	5	5
Mg^{2+}	1.5	1.5
Ca^{2+}	2.5	2.5
Cl^-	103	147.8
HCO_3^-	27	4.2
HPO_4^{2-}	1	1
SO_4^{2-}	0.5	0.5
pH	7.2–7.4	7.40

chemical properties were calculated from PDS curves using the Tafel method. The corrosion current density (I_{corr}) and corrosion potential (E_{corr}) were determined from the intersection of linear portions of the anodic (β_a) and cathodic (β_c) Tafel slopes (Ref 34). Tafel parameters, corrosion rates, and polarization resistances were all determined using Gamry Echem Analyst software.

2.7 SEM-EDS and XRD Analysis

Surface morphologies of the coated samples were characterized with scanning electron microscopy (SEM, Hitachi SU3500) at various scales. Energy-dispersive X-ray spectroscopy (EDS, Oxford INCA X-ray spectrometer) was performed for the scanned regions. Additionally, XRD analyses (Rigaku MiniFlex-600) were conducted at a wavelength of 1.5406 (λ) between 10 and 90° with a step speed of 0.02°.

3. Results and Discussion

The results from and discussions regarding boron-hydroxyapatite biocomposite synthesis, the characterization and staging, and the coating of NiTi substrates using EPD are given below under separate headings.

3.1 Structural Characterization of Boron-Doped Bioceramic Powders

The synthesized bioceramic powders containing 5, 10, and 15 wt.% boron-doped hydroxyapatite (B-HAp) were sintered at 1000°C for 2 h, then morphologically characterized by using XRD and FT-IR. Figure 1 shows the combined XRD spectra of both boron-doped (5, 10, and 15 wt.%) and HAp-only powders. The analysis was performed to investigate possible phase transformation of the coatings after the sintering process at 1000°C. The characteristics peaks of the HAp were observed in a wider area between the 30-34° 2θ values in the diffractogram of the coatings. It was evident from the peaks that the addition of boron led to a partial deterioration of the HAp structure and transformation of HAp to tricalcium phosphate (TCP). In other words, the structural integrity of HA was partly decomposed with sintering, and Ca and P elements transform into different compounds. This is consistent with previous reports that the presence of boron during the synthesis phase causes some degradation in HAp structure after sintering and increased proportions of boron cause TCP formation (Ref 35, 36). The XRD results of the present study indicate that the boron-doped HAp composite structure formed differently from those characterized by Ternane et al. (Ref 12), in which peak intensity increased with increasing boron addition. However, the B_2O_3 structures identified in the 2θ range at 29.9° coincide with those identified by Kohoshima et al. (Ref 37) in a study that synthesized B_2O_3-HAp biocomposites of various proportions.

The FT-IR analysis results of the coated samples are presented in Fig. 2. The presence of boron in the obtained biocomposite structures was confirmed in both BO3-3 and BO2- peaks being detected through the analysis. In some previous studies (Ref 12, 36, 38), BO_3^{-3} peaks were detected at wavelengths of 744, 770, 783, and 1304, 1254, 1204 cm^{-1}, while BO_2^- peaks were detected at 1993 and 2000 cm^{-1}. The peaks obtained in this study were consistent with the results reported in the literature. Besides, the presence of hydroxyapatite phases is verified with bands in the numbers of 1000-1050 and 550-650 cm^{-1} wavenumber (Ref 24). With the increase in B addition, peak intensity changes in the phosphate group occurred in the coating layer applied on NiTi.

3.2 Morphological Characterization of Bioceramic Coatings

SEM surface images of the only-HAp, 5, 10, and 15 wt.% B-doped HAp powders coated on NiTi substrates are depicted in Fig. 3(a-d), respectively. It was observed that all coatings have small voids. However, macro cracks or delamination were not observed in coating layers after sintering. However, macro cracks or delamination were not observed in coating layers after sintering. The 5 and 15 wt.% B-HAp biocomposites both achieved homogenous coatings; however, regional differences were observed in the only-HAp and 10 wt.% B-HAp coatings. These results reveal the importance of the proportion of boron used in the biocomposite. EDS (Fig 3b-d) revealed added boron
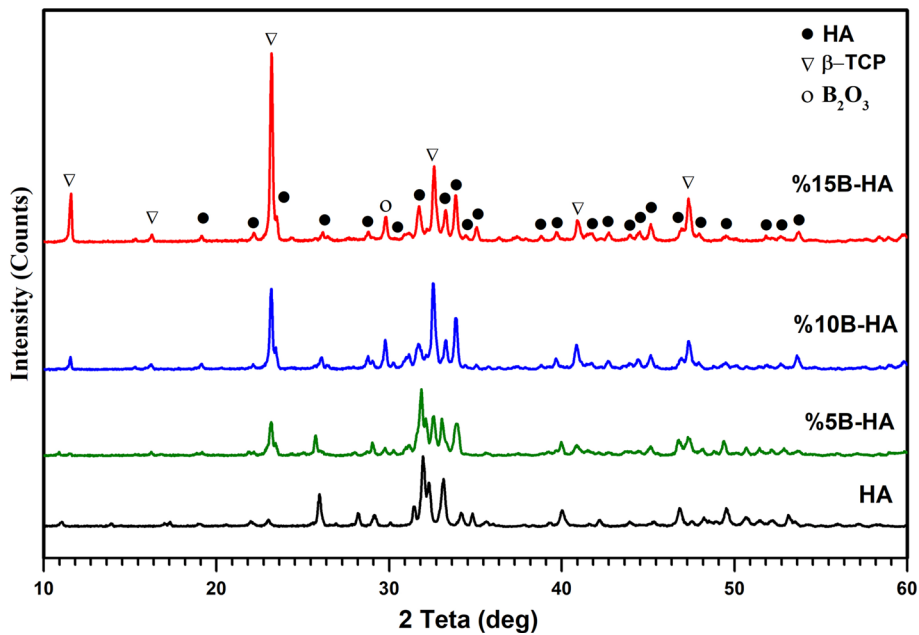
Fig. 1 XRD spectra of HAp and B-doped HAp biocomposite coatings (5, 10, and 15% B)
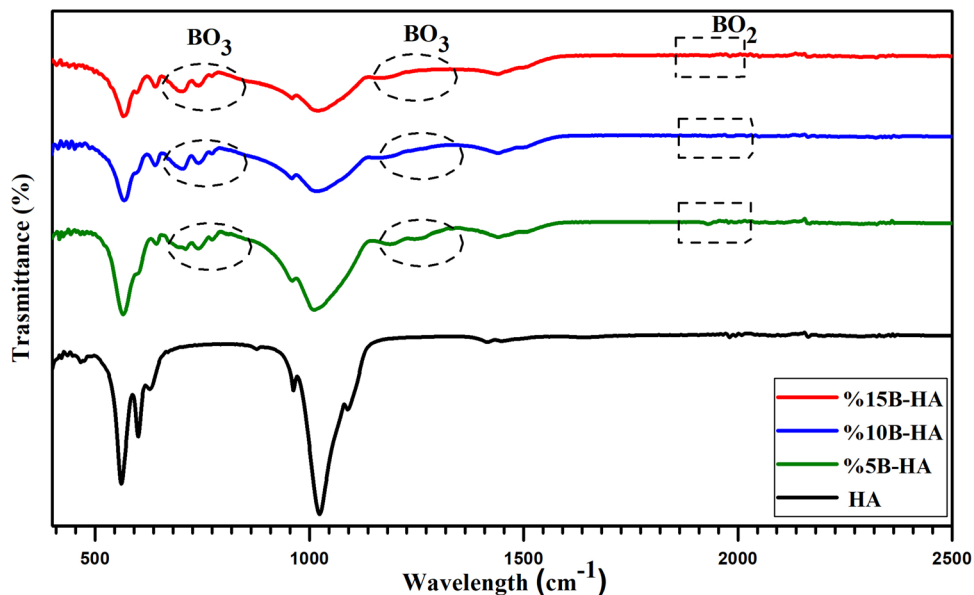

Fig. 2 Fourier-transform infrared spectra of HAp and B-doped HAp biocomposite coatings (5, 10, and 15% B)

to result in better interconnections being formed between grains and pores; the best inter-grain bonds were observed in 15 wt.% B-HAp biocomposite coatings (Fig 3d), while poor bonding was observed with both only-HAp (Fig. 3a) and 5 wt.% B-HAp (Fig 3b).

Table 1 presents the average coating film thicknesses (μm) of some NiTi sample groups. The thinnest coating was obtained for the N_1 sample (only-HAp, 60 s), while the thickest coating belonged to the N_{12} sample (15 wt.% B-HAp, 120 s). Film thickness depended on coating time and the proportion of boron. Notably, coatings constructed with the only-HAp, 5 wt.%, and 10 wt.% B-HAp powders exhibited a linear increase in thickness with increased deposition duration. In contrast, the 15 wt.% B-HAp coating exhibited a significant increase above

the 90 s deposition time. The deposition was also improved by the addition of boron and iodine due to each increasing conductivity of the EPD suspension, which led to increased particle charge and thus improved deposition. Figure 4 shows the deposit weight per unit area (mg/cm^2) of the various coatings

There is no consensus in the literature on the optimum thickness range for coatings applied to biomaterials. Herrera *et al.* (Ref 39) state that HAp with a thickness of 10-15 μm can dissolve quickly in tissues, but coatings of 100-150 μm can break and come loose, especially when exposed to the forces formed in hard tissues. The coating thicknesses obtained in this study (23-76.5 μm) were intermediate between these reported values.
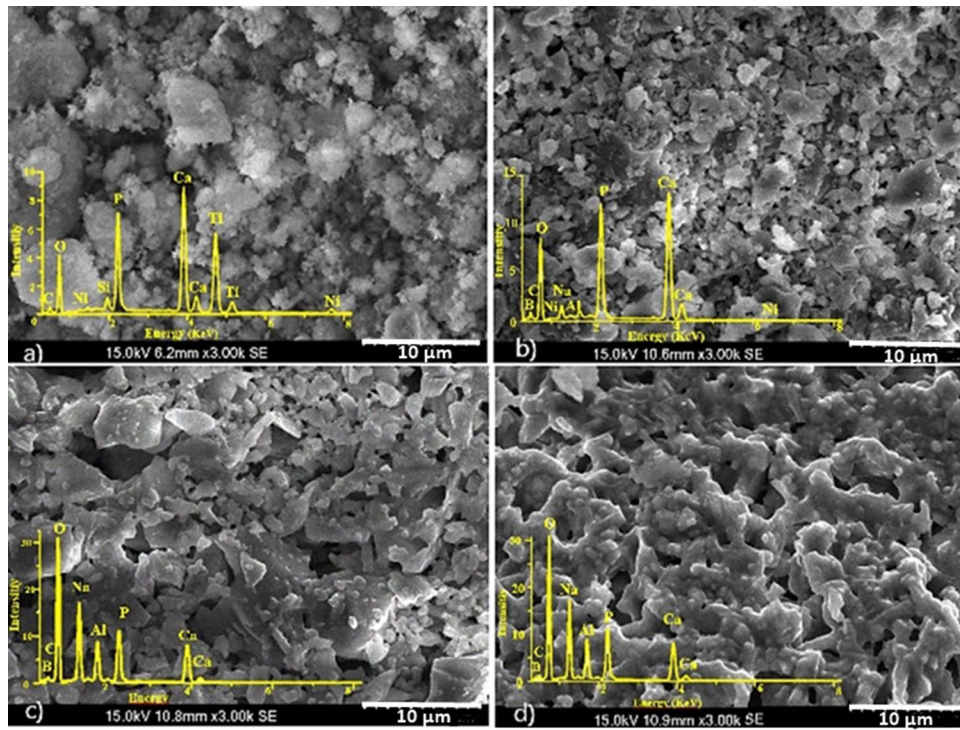
Fig. 3 SEM images and EDS spectra of biocomposite-coated NiTi before corrosion: (a) only-HAp (N_1), (b) 5% B-HAp (N_6), (c) 10% B-HAp (N_9), and (d) 15% B-HAp (N_{12})
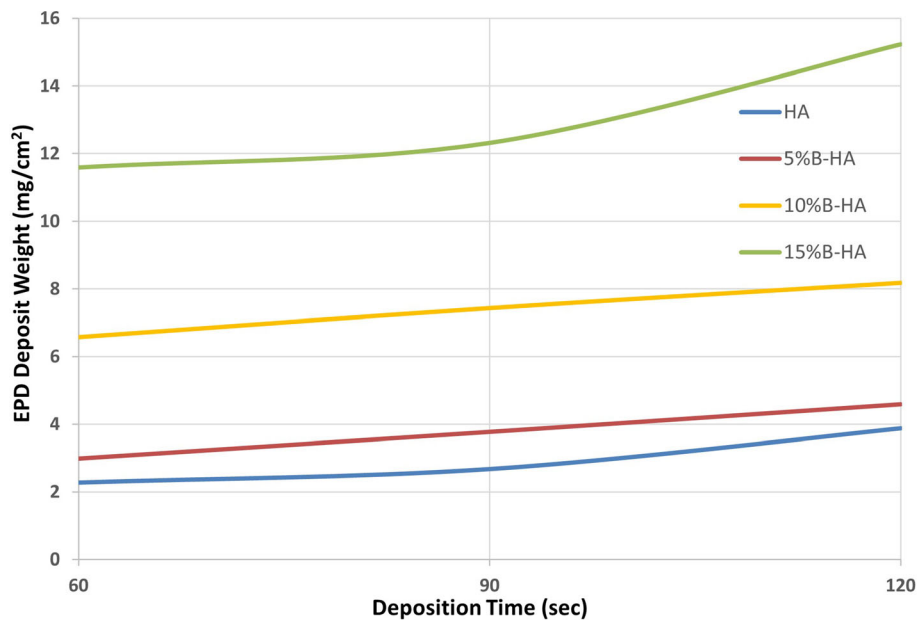

Fig. 4 Change in deposit weight with deposition time for coating groups

3.3 Adhesion Strength

Pull-out tests were performed to determine the adhesion strength of the interfaces between NiTi substrates and deposited coatings, which is the most important factor affecting the adhesion strength of the coating. Initially, uncoated NiTi substrates were tested to determine the adhesion strength of the epoxy, which was 36 MPa. Figure 5 depicts the adhesion strengths of the various coatings in the context of film thickness.

Figure 5 compares sample groups in terms of coating thickness, deposition time, and associated changes in adhesion strength. The lowest adhesion strength (16 MPa) was obtained for only-HAp with 120 s deposition time (N_3), while the highest adhesion strength (30 MPa) was obtained for 15 wt.% B-HAp with 90 s deposition time (N_{11}). Overall, among only-HAp coatings (N_1, N_2, N_3), coating thickness increased but adhesion strength decreased with increasing deposition time. Meanwhile, the 5, 10, and 15 wt.% B–HAp powders (N_4-N_{12})
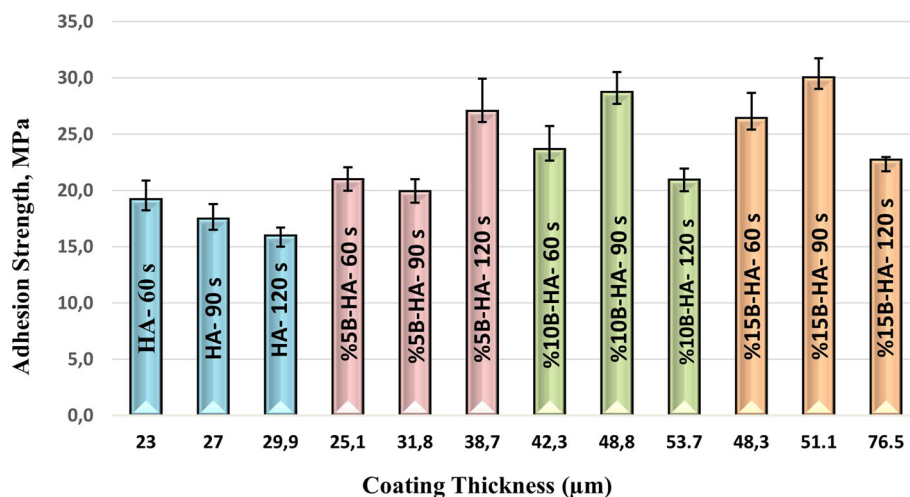
Fig. 5 1Coating thickness, deposition time, and adhesion strength changes for coating groups

exhibited greater adhesion strength than did the only-HAp coatings (N_1, N_2, N_3). However, no standard trend was found relating coating thickness to adhesion strength. Although up to 58.8% thicker films were obtained with B-HAp coatings (N_4-N_{12}), boron addition caused only about a 30% to 50% increase in adhesion strength. The factors influencing coating adhesion can only be elucidated when adhesion strengths and SEM images are considered together. In particular, the surface morphology of N_{11} (Fig. 3d) allowed for better coating and sintering than N_1 (Fig. 3a), thus better bonds between B and HAp powders and so higher adhesion values being attained by N_{11}.

Some researchers have applied HAp-TiO_2 and HAp-ZrO_2 composite coatings to NiTi substrates, obtaining respective adhesion strengths of 23.7 and 24.2 MPa. The adhesion strength results in the present study are higher than similar studies in the literature that have used reinforced HAp (40-43).

3.4 In-vitro Corrosion Results

Figure 6 shows the open circuit potential (E_{ocp}) curves obtained for the coated NiTi samples in SBF. A waiting period of 30 min was employed to allow samples to become stable in the corrosion environment. Except for the N_1, N_2, and N_{12} sample groups, initial tests of samples showed more active values (negative potentials), which caused superficial corrosion. For the N_1 and N_7 samples, the steady-state OCP potential differed significantly from the initial potential. In addition, as seen from the figure, some irregular fluctuations were detected while reaching a steady-state, reactions occurred on sample surfaces, and pitting corrosion occurred when passivation was eliminated.

Potentiodynamic scanning (PDS) was performed after open circuit potentials (OCP) became stable (Fig. 7). Table 3 gives the corrosion parameters extrapolated from PDS curves using the Tafel method. Protecting a metallic implant from corrosion requires a nobler corrosion potential (E_{corr}) and a lower corrosion current (I_{corr}). Notably, the only-HAp coatings (N_1, N_2) exhibited decreased corrosion resistance relative to un-coated NiTi samples. Improved corrosion values were likewise not achieved for the 5 wt.% boron-doped HAp coatings (N_5, N_6). In contrast, the 10 wt.% B-HAp coated N_7 and N_{12} samples both exhibited decreased corrosion rate and high

corrosion resistance, indicating that such coatings increase corrosion resistance. Overall, the N_{12} samples (15 wt.% B-HAp, 120 s deposition) yielded the best corrosion resistance out of all uncoated and coated formulations. The fluctuation is observed in E_{ocp} curve of N12 sample. As it is known that, the coating was typically permeable to ions at the beginning of the submerging of the sample in the electrolyte, and the E_{ocp} was decreased fast due to the different barrier properties of the coating such as higher B content. However, this permeability took a longer time than other samples due to the higher thickness of the sample than the others as given in Table 1. Probably, the E_{ocp} has increased again due to the passivation of the substrate after the electrolyte and reached to the underlayer of the coated substrate. Zhang *et al.* (Ref 43) similarly coated NiTi with GO (graphene oxide) using the EPD method and also reported lower I_{corr} values and increased corrosion resistance relative to uncoated NiTi.

3.5 Comparison of Coatings Before and After Corrosion Tests

Biological corrosion is among the undesirable surface problems encountered when NiTi alloys are used in extreme load and biologically aggressive environments, e.g., body fluid. As body fluid contains water, dissolved oxygen, protein, and chloride and hydroxide ions, this biological environment is highly corrosive for the metals and metal-based alloys used as biomaterials (Ref 43, 44).

Figure 8(a-d) presents the SEM surface images and EDS spectra of coated NiTi samples. Overall, surface pitting was observed for samples coated with either only-HAp (Fig. 8a) or 5 wt.% B-HAp (Fig. 8b), whereas higher proportions of boron resulted in less corrosion damage. The EDS spectra of all four sample groups exhibit decreased Ca, P, and B content post-exposure, which indicates corrosive damage to the coating, and also exhibits a significant reduction in NiTi signal. It is likewise evident from the XRD spectra that oxidation in the substrate increased (Fig. 9), and the presence of rutile (TiO_2) and Ni_3Ti in post-corrosion spectra (Fig. 10) indicates that corrosion reached the substrate and caused damage.

It must be noted that the high carbon (C) percentages in the EDS analyses are due to the polyester in the Bakelite on which samples were placed for corrosion tests. Likewise, the presence
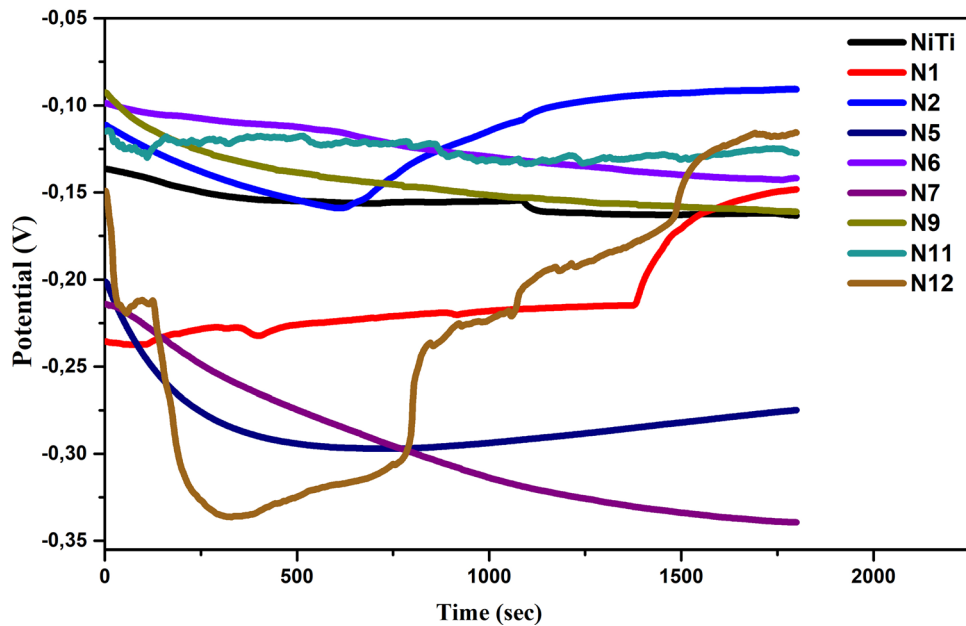
Fig. 6 Open circuit potential (OCP) curves of biocomposite coating groups on NiTi
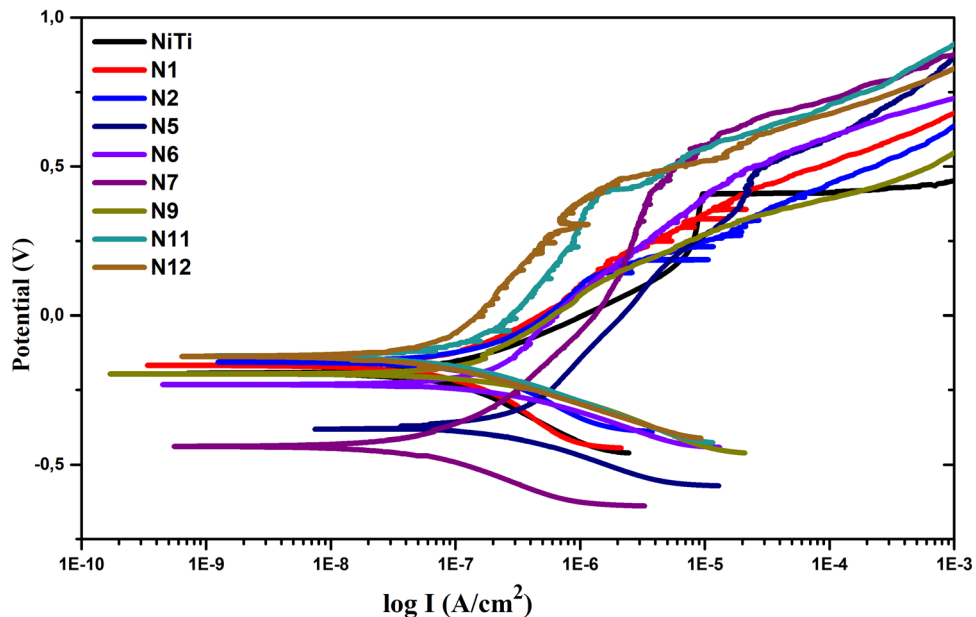

Fig. 7 Comparison of potentiodynamic scanning (PDS) curves with different B-doping proportions (wt.%) and deposition times

of Na is due to the NaOH used as a pH regulator in the production of biocomposite powders, while the observed Al signals represent contamination from the mortar (Al_2O_3) used for grinding biocomposite powders that coagulated after sintering. Finally, the detection of Si indicates that a slight amount of the silica sand (SiO_2) used in the sandblasting process remained on the surface even after cleaning.

Regarding the specific performance of coatings, the only-HAp and 5% B-HAp coated samples both exhibited homogeneous morphologies before corrosion (Fig. 3a-b) but were severely damaged after exposure, with large-scale pitting (Fig. 8a-b). Interestingly, the 5 wt.% B-HAp coatings were subjected to more corrosion than the only-HAp coatings; the pitting of that sample was so extensive that coating materials

(Ca, P, and B) were not even present in the post-corrosion EDS analysis, with only substrate atoms (Ni and Ti) being identified in the pitted area. Similarly, decreased XRD 2θ peak intensities of coating materials (25.8, 31.5, 33, 34 and 49.2°) and increased signal from NiTi (2θ=42.3-43), Ni_3Ti (2θ=46.3), and TiO_2 (2θ=41.2) structures are evidence of severe corrosion damage. The primary reason for the greater susceptibility of 5 wt.% B-HAp to corrosion may be the greater number of pores and cracks and the poor inter-grain bonds obtained during coating. Regional cracks or areas of weak bonding that formed during the sintering process allowed corrosion to progress, resulting in deeper pitting on the surface of the metallic substrate. Kwok *et al.* (Ref 44) also reported that the presence of cracks and pores in a coating film does not constitute an

Table 3 Corrosion parameters calculated from PDS curves of the coatings

ID	E_{ocp}, mV	E_{corr}, mV	I_{corr}, nA·cm^{-2}	Corr. rate, mpy	R_p, ×10^3, ohms.cm^2
Uncoated NiTi	−163	−193	119	0.055	418
N$_1$	**−148**	**−167**	**145**	**0.067**	**487**
N$_2$	−91	−154	251	0.116	302
N$_3$	−92	−183	256	0.119	151
N$_4$	−266	−277	147	0.683	48
N$_5$	−274	−381	293	0.136	189
N$_6$	−142	−231	161	0.074	242
N$_7$	−399	**−438**	**110**	0.051	**600**
N$_8$	−220	−261	141	0.065	295
N$_9$	**−161**	**−195**	**100**	**0.046**	**326**
N$_{10}$	−95	−129	186	0.086	247
N$_{11}$	−127	−136	149	0.069	372
N$_{12}$	**−112**	**−138**	**79**	**0.036**	**597**
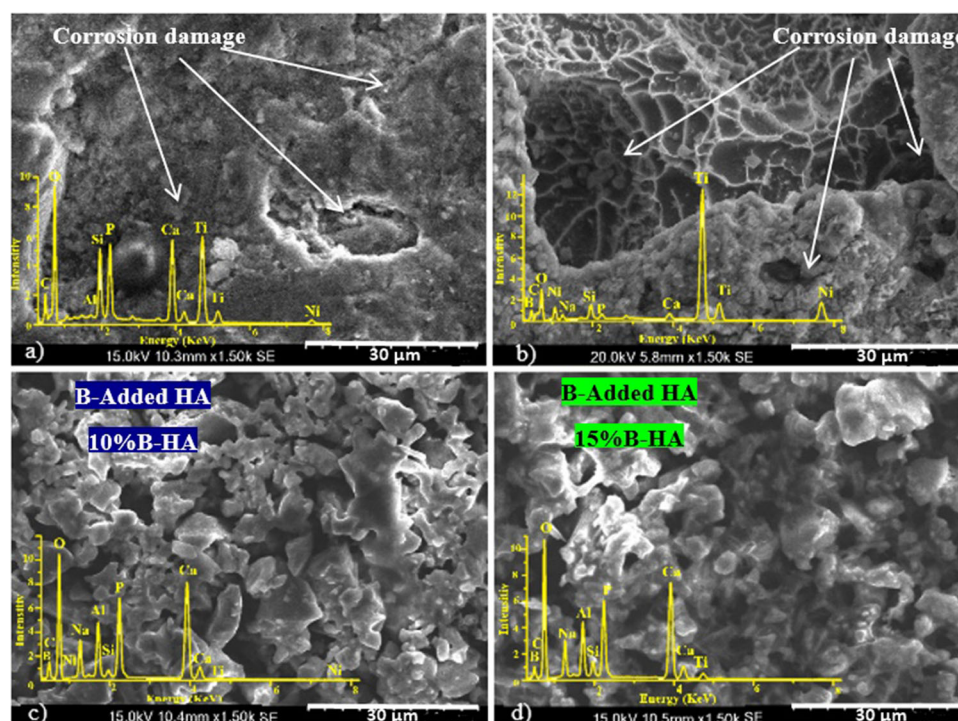
Fig. 8 SEM images and EDS spectra of biocomposite-coated NiTi after corrosion: (a) only-HAp (N$_1$), (b) 5% B-HAp (N$_6$), (c) 10% B-HAp (N$_9$), and (d) 15% B-HAp (N$_{12}$)

obstacle to corrosion, and decreases the corrosion resistance of metallic substrates.

The N$_{10-12}$ sample groups likewise exhibited homogenous coating surfaces before exposure (Fig. 3b-d), which surfaces were not greatly affected by corrosion (Fig. 8c). The pre-corrosion (Fig 3c) and post-corrosion (Fig 8c) EDS spectra show that the 10 wt.% B-HAp biocomposite coating exhibited only slight decreases in surface Ca, P, and B content and slight increases in substrate content (Ni, Ti), findings also supported by XRD analyses. These results indicate that corrosion did reach the substrate under 10 wt.% B-HAp coatings, although surface damage was minimal. Meanwhile, the N$_7$ and N$_{12}$ groups demonstrated I_{corr} and E_{corr} values close to zero (Table 3) and XRD analysis results (Fig. 10c-d) that indicate high corrosion resistance.

As with other coated samples, the 15 wt.% boron-doped HAp biocomposite coatings exhibited homogeneous surfaces pre-corrosion, especially for N$_9$ (Fig. 3c-d). Unlike other coating types, post-corrosion SEM images (Fig 8c-d) did not show any significant damage to the surfaces. However, the EDS and XRD spectra revealed increased Ca and P proportions, a 50% decrease in boron content, and minimal increases in NiTi peak intensities (Fig. 10d-f), which results indicate that corrosion affected the substrate.

In light of the increased corrosion resistance and adhesion strength identified from the present findings, it is predicted that biocomposite-coated materials such as those obtained in this study, particularly 15% wt.% B-HAp, may open up new applications in the biomedical field and extend the life of implants in the body.
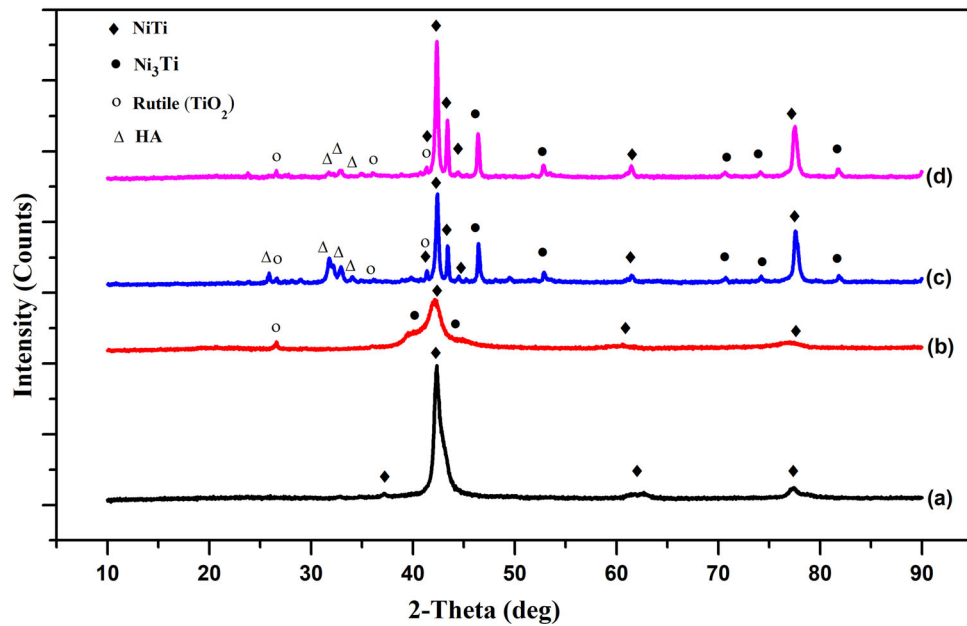
Fig. 9 XRD spectra of uncoated NiTi (a) pre-corrosion and (b) post-corrosion, and of only-HAp coated NiTi (c) pre-corrosion and (d) post-corrosion
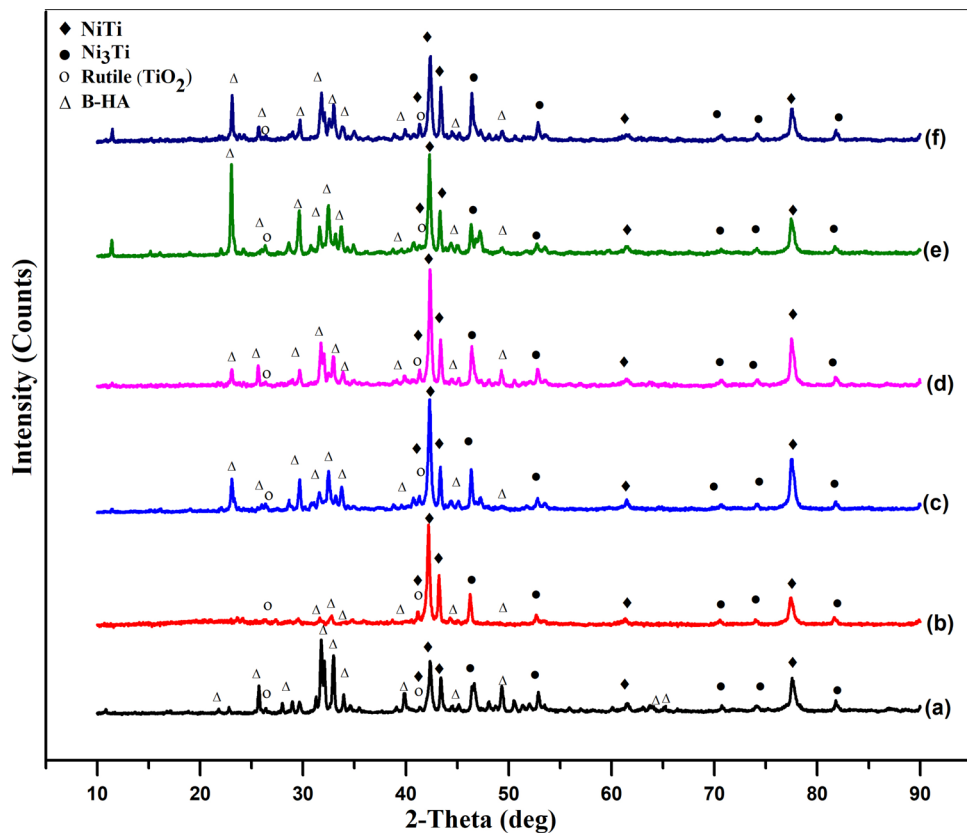

Fig. 10 XRD spectra of NiTi samples with boron-doped coatings: 5 wt.% B-HAp (a) pre-corrosion and (b) post-corrosion, 10 wt% B-HAp (c) pre-corrosion and (d) post-corrosion, and 15 wt.% B-HAp e pre-corrosion and (f) post-corrosion

4. Conclusions

Hydroxyapatite (HAp) and boron-doped hydroxyapatite (B-HAp) composite powders were synthesized using the sol-gel method and used to coat NiTi metallic surfaces via EPD in the interest of improving implant mechanical properties and corrosion resistance. The key findings can be summarized as follows:

- The best surface morphology, adhesion strength, and corrosion resistance were obtained when sintering with the optimized parameters of 750 °C, 75 mins, and 3 °C·min^{-1} sintering rate.
- Iodine in EPD suspensions provided a better deposition rate and a more homogeneous coating surface, helping to enhance adhesion and so corrosion resistance.
- For only-HAp coating, adhesion strength decreased as coating thickness increased; however, across all groups, no distinct correlation was identified between film thickness and adhesion.
- The addition of boron as a reinforcement to HAp provided a more homogeneous coating, improved surface morphology, and increased adhesion between grains, resulting in a crack-free and porous surface.
- Among B-reinforced coatings, 10 wt.% B-HAp (N_7) and 15 wt.% B-HAp (N_9 and N_{12}) biocomposite coatings provided better corrosion resistance. The greatest adhesion strength (30 MPa) was achieved for 15 wt.% B-HAp with 120 s deposition time (N_{12}).

References

1. K.M.R. Nuss and B. von Rechenberg, Biocompatibility Issues with Modern Implants in Bone-A Review for Clinical Orthopedics, *Open Orthop. J.*, 2008, **2**(1), p 66–78. https://doi.org/10.2174/1874325000802010066

2. A.F. Mavrogenis, R. Dimitriou, J. Parvizi, and G.C. Babis, Biology of Implant Osseointegration. *J. Musculoskelet. Neuronal Interact.*, n.d., 2009, **9**(2), p 61–71. http://www.ncbi.nlm.nih.gov/pubmed/19516081

3. B. Dikici, Z. Esen, O. Duygulu, and S.G. (Koc), Corrosion of Metallic Biomaterials, *Advances in Metallic Biomaterials: Tissues, Materials and Biological Reactions*, M. Niinomi, T. Narushima, and M. Nakai, Eds., (Berlin, Heidelberg), Springer-Verlag Berlin Heidelberg, (2015), p 275–303, doi:https://doi.org/10.1007/978-3-662-46836-4

4. M. Geetha, A.K. Singh, R. Asokamani and A.K. Gogia, Ti Based Biomaterials, the Ultimate Choice for Orthopaedic Implants–A Review, *Prog. Mater. Sci.*, 2009, **54**(3), p 397–425. https://doi.org/10.1016/j.pmatsci.2008.06.004

5. E. Ergun, C. Elmas, and N.E. Olcay, "Properties of Bioceramics Materials and Their Applications," *10th Denizli Mater Symp and Exhibition*, (Denizli, Turkey), Pamukkale Üniversitesi, (2004), p 25–41

6. T.W. Duerig, K.N. Melton and J.L. Proft, Wide Hysteresis Shape Memory Alloys, *Engineering Aspects of Shape Memory Alloys*, 1990 https://doi.org/10.1016/B978-0-7506-1009-4.50015-9

7. B. O'Brien, F.M. Weafer and M.S. Bruzzi, Shape Memory Alloys for Use in Medicine, *Comprehensive Biomaterials II*, *Elsevier*, 2017 https://doi.org/10.1016/B978-0-12-803581-8.10084-0

8. D.M. Brunette, P. Tengvall, M. Textor, and P. Thomsen, "Titanium in Medicine: Material Science, Surface Science, Engineering, Biological Responses and Medical Applications," (Berlin, Heidelberg), Springer Berlin Heidelberg, (2001), doi:https://doi.org/10.1007/978-3-642-56486-4

9. H. Huang, Ion Release from NiTi Orthodontic Wires in Artificial Saliva with Various Acidities, *Biomaterials*, 2003, **24**(20), p 3585–3592. https://doi.org/10.1016/S0142-9612(03)00188-1

10. B. Aksakal, M. Kom, H.B. Tosun and M. Demirel, Influence of Micro- and Nano-Hydroxyapatite Coatings on the Osteointegration of Metallic (Ti6Al4 V) and Bioabsorbable Interference Screws: An in Vivo Study, *Eur. J. Orthop. Surg. Traumatol.*, 2014, **24**(5), p 813–819. https://doi.org/10.1007/s00590-013-1236-8

11. Y. Say and B. Aksakal, Effects of Hydroxyapatite/Zr and Bioglass/Zr Coatings on Morphology and Corrosion Behaviour of Rex-734 Alloy, *J. Mater. Sci. Mater. Med.*, 2016, **27**(6), p 105. https://doi.org/10.1007/s10856-016-5716-3

12. R. Ternane, M.T. Cohen-Adad, G. Panczer, C. Goutaudier, N. Kbir-Ariguib, M. Trabelsi-Ayedi, P. Florian and D. Massiot, Introduction of Boron in Hydroxyapatite: Synthesis and Structural Characterization, *J. Alloys Compd.*, 2002, **333**(1–2), p 62–71. https://doi.org/10.1016/S0925-8388(01)01558-4

13. S.S. Hakki, B.S. Bozkurt and E.E. Hakki, Boron Regulates Mineralized Tissue-Associated Proteins in Osteoblasts (MC3T3-E1), *J. Trace Elem. Med. Biol.*, 2010, **24**(4), p 243–250. https://doi.org/10.1016/j.jtemb.2010.03.003

14. A.E. Pazarçeviren, A. Tezcaner, D. Keskin, S.T. Kolukısa, S. Sürdem and Z. Evis, Boron-Doped Biphasic Hydroxyapatite/β-Tricalcium Phosphate for Bone Tissue Engineering, *Biol. Trace Elem. Res.*, 2021, **199**(3), p 968–980. https://doi.org/10.1007/s12011-020-02230-8

15. T.A. Devirian and S.L. Volpe, The Physiological Effects of Dietary Boron, *Crit. Rev. Food Sci. Nutr.*, 2003, **43**(2), p 219–231. https://doi.org/10.1080/10408690390826491

16. B. Dikici, M. Niinomi, M. Topuz, Y. Say, B. Aksakal, H. Yilmazer and M. Nakai, Synthesis and Characterization of Hydroxyapatite/TiO2 Coatings on the β-Type Titanium Alloys with Different Sintering Parameters Using Sol-Gel Method, *Prot. Met. Phys. Chem. Surfaces*, 2018, **54**(3), p 457–462. https://doi.org/10.1134/S2070205118030255

17. Y. Say, B. Aksakal and B. Dikici, Effect of Hydroxyapatite/SiO2 Hybride Coatings on Surface Morphology and Corrosion Resistance of REX-734 Alloy, *Ceram Int.*, 2016, **42**(8), p 10151–10158

18. B. Aksakal, Y. Say, Ç. Buyukpinar and S. Bakirdere, Biodegradation of Hydroxyapatite Coated Rex-734 Alloy with Silver and Selenium/Chitosan Substitutions, *Vitro Analysis. Ceram. Int.*, 2017, **43**(15), p 12609–12615

19. N. Aslan and B. Aksakal, Effect of Graphene Reinforcement on Hybrid Bioceramic Coating Deposited on the Produced Porous Ti64 Alloys, *J. Porous Mater.*, 2021 https://doi.org/10.1007/s10934-021-01081-5

20. G. Feng, X. Cheng, D. Xie, K. Wang and B. Zhang, Fabrication and Characterization of Nano Prism-like Hydroxyapatite Coating on Porous Titanium Substrate by Combined Biomimetic-Hydrothermal, *Method. Mater. Lett*, 2016, **163**, p 134–137. https://doi.org/10.1016/j.matlet.2015.10.063

21. M. Mehrali, A.R. Akhiani, S. Talebian, M. Mehrali, S.T. Latibari, A. Dolatshahi-Pirouz, and H.S.C. Metselaar, Electrophoretic Deposition of Calcium Silicate-Reduced Graphene Oxide Composites on Titanium Substrate, *J. Eur. Ceram. Soc.*, (2016)

22. B. Wu, S. Xiong, Y. Guo, Y. Chen, P. Huang and B. Yang, Tooth-Colored Bioactive Titanium Alloy Prepared with Anodic Oxidation Method for Dental Implant Application, *Mater. Lett.*, 2019, **248**, p 134–137. https://doi.org/10.1016/j.matlet.2019.04.015

23. L. Zhang, W. Liu, C. Yue, T. Zhang, P. Li, Z. Xing and Y. Chen, A Tough Graphene Nanosheet/Hydroxyapatite Composite with Improved in Vitro Biocompatibility, *Carbon N.*, 2013, **61**, p 105–115. https://doi.org/10.1016/j.carbon.2013.04.074

24. O. Yigit, B. Dikici, T.C. Senocak and N. Ozdemir, One-Step Synthesis of Nano-Hydroxyapatite/Graphene Nanosheet Hybrid Coatings on Ti6Al4V Alloys by Hydrothermal Method and Their in-Vitro Corrosion Responses, *Surf. Coatings Technol.*, 2020, **394**, p 125858. https://doi.org/10.1016/j.surfcoat.2020.125858

25. F. Songur, B. Dikici, M. Niinomi and E. Arslan, The Plasma Electrolytic Oxidation (PEO) Coatings to Enhance in-Vitro Corrosion Resistance of Ti–29Nb–13Ta–4.6Zr Alloys: The Combined Effect of Duty Cycle and the Deposition Frequency, *Surf. Coatings Technol.*, 2019, **374**, p 345–354. https://doi.org/10.1016/j.surfcoat.2019.06.025

26. B. Aksakal and A.R. Boccaccini, Electrophoretic Deposition of Selenium, *Mater. Lett.*, 2012, **76**, p 177–180. https://doi.org/10.1016/j.matlet.2012.02.059

27. E. Mohseni, E. Zalnezhad and A.R. Bushroa, Comparative Investigation on the Adhesion of Hydroxyapatite Coating on Ti–6Al–4V Implant: A Review Paper, *Int. J. Adhes. Adhes.*, 2014, **48**, p 238–257. https://doi.org/10.1016/j.ijadhadh.2013.09.030

28. X. Meng, T.-Y. Kwon, Y. Yang, J.L. Ong and K.-H. Kim, Effects of Applied Voltages on Hydroxyapatite Coating of Titanium by Electrophoretic Deposition, *J. Biomed. Mater. Res. Part B Appl. Biomater.*, 2006 https://doi.org/10.1002/jbm.b.30497

29. Y. Göncü, M. Geçgin, F. Bakan and N. Ay, Electrophoretic Deposition of Hydroxyapatite-Hexagonal Boron Nitride Composite Coatings on Ti Substrate, *Mater. Sci. Eng. C*, 2017, **79**, p 343–353. https://doi.org/10.1016/j.msec.2017.05.023

30. A. Jemat, M.J. Ghazali, M. Razali and Y. Otsuka, Surface Modifications and Their Effects on Titanium Dental Implants, *Biomed Res. Int.*, 2015, **2015**, p 1–11. https://doi.org/10.1155/2015/791725

31. A. Wennerberg, C. Hallgren, C. Johansson, and S. Danelli, A Histomorphometric Evaluation of Screw-Shaped Implants Each Prepared with Two Surface Roughnesses, *Clin. Oral Implants Res.*, (1998)

32. H. Farnoush, G. Aldıç and H. Çimenoğlu, Functionally Graded HA–TiO2 Nanostructured Composite Coating on Ti–6Al–4V Substrate via Electrophoretic Deposition, *Surf. Coatings Technol.*, 2015, **265**, p 7–15

33. T. Kokubo and H. Takadama, How Useful Is SBF in Predicting in Vivo Bone Bioactivity?, *Biomaterials*, 2006, **27**(15), p 2907–2915. https://doi.org/10.1016/j.biomaterials.2006.01.017

34. S. Papavinasam, Electrochemical Polarization Techniques for Corrosion Monitoring, *Techniques for Corrosion Monitoring*, 2008 https://doi.org/10.1533/9781845694050.1.49

35. O. Albayrak and M. Ugurlu, Preparation and Characterization of Boron Doped Hydroxyapatite: Effects of Boron Content and Sintering Temperature on Structure and Mechanical Properties, *Gazi Üniversitesi Mühendislik-Mimarlık Fakültesi Derg.*, 2016 https://doi.org/10.17341/gummfd.59636

36. H. Güler, G. Gündoğmaz, F. Kurtuluş, G. Çelik and ŞS. Gacanoğlu, Solid State Synthesis of Calcium Borohydroxyapatite, *Solid State Sci.*, 2011, **13**(11), p 1916–1920. https://doi.org/10.1016/j.solidstatesciences.2011.08.016

37. S. Khoshsima, A. Alshemary, A. Tezcaner, S. Surdem and Z. Evis, Impact of B2O3 and La2O3 Addition on Structural, Mechanical and Biological Properties of Hydroxyapatite, *Process. Appl. Ceram.*, 2018, **12**(2), p 143–152. https://doi.org/10.2298/PAC1802143K

38. O. Albayrak, Structural and Mechanical Characterization of Boron Doped Biphasic Calcium Phosphate Produced by Wet Chemical Method and Subsequent Thermal Treatment, *Mater. Charact.*, 2016, **113**, p 82–89. https://doi.org/10.1016/j.matchar.2016.01.006

39. A. Herrera, J. Mateo, J. Gil-Albarova, A. Lobo-Escolar, E. Ibarz, S. Gabarre, Y. Más and L. Gracia, Cementless Hydroxyapatite Coated Hip Prostheses, *Biomed. Res. Int.*, 2015, **2015**, p 1–13. https://doi.org/10.1155/2015/386461

40. D. Qiu, A. Wang and Y. Yin, Characterization and Corrosion Behavior of Hydroxyapatite/Zirconia Composite Coating on NiTi Fabricated by Electrochemical Deposition, *Appl. Surf. Sci.*, 2010, **257**(5), p 1774–1778. https://doi.org/10.1016/j.apsusc.2010.09.014

41. D. Qiu, L. Yang, Y. Yin and A. Wang, Preparation and Characterization of Hydroxyapatite/Titania Composite Coating on NiTi Alloy by Electrochemical Deposition, *Surf. Coatings Technol.*, 2011, **205**(10), p 3280–3284

42. H. Maleki-Ghaleh, V. Khalili, J. Khalil-Allafi and M. Javidi, Hydroxyapatite Coating on NiTi Shape Memory Alloy by Electrophoretic Deposition Process, *Surf. Coatings Technol.*, 2012, **208**, p 57–63. https://doi.org/10.1016/j.surfcoat.2012.08.001

43. K. Zhang, H. Zhang, P. Liu, C. Zhang, W. Li, X. Chen and F. Ma, Electrophoretic Deposition of Graphene Oxide on NiTi Alloy for Corrosion Prevention, *Vacuum*, 2019, **161**, p 276–282. https://doi.org/10.1016/j.vacuum.2018.12.032

44. C.T. Kwok, P.K. Wong, F.T. Cheng and H.C. Man, Characterization and Corrosion Behavior of Hydroxyapatite Coatings on Ti6Al4V Fabricated by Electrophoretic Deposition, *Appl. Surf. Sci.*, 2009, **255**(13–14), p 6736–6744